

# Epithelium segmentation using deep learning in H&E-stained prostate specimens with immunohistochemistry as reference standard

Wouter Bulten, Péter Bándi, Jeffrey Hoven, Rob van de Loo, Johannes Lotz, Nick Weiss, Jeroen van der Laak, Bram van Ginneken, Christina Hulsbergen-van de Kaa, Geert Litjens

**Abstract**—Prostate cancer (PCa) is graded by pathologists by examining the architectural pattern of cancerous epithelial tissue on hematoxylin and eosin (H&E) stained slides. Given the importance of gland morphology, automatically differentiating between glandular epithelial tissue and other tissues is an important prerequisite for the development of automated methods for detecting PCa. We propose a new method, using deep learning, for automatically segmenting epithelial tissue in digitized prostatectomy slides. We employed immunohistochemistry (IHC) to render the ground truth less subjective and more precise compared to manual outlining on H&E slides, especially in areas with high-grade and poorly differentiated PCa. Our dataset consisted of 102 tissue blocks, including both low and high grade PCa. From each block a single new section was cut, stained with H&E, scanned, restained using P63 and CK8/18 to highlight the epithelial structure, and scanned again. The H&E slides were co-registered to the IHC slides. On a subset of the IHC slides we applied color deconvolution, corrected stain errors manually, and trained a U-Net to perform segmentation of epithelial structures. Whole-slide segmentation masks generated by the IHC U-Net were used to train a second U-Net on H&E. Our system makes precise cell-level segmentations and segments both intact glands as well as individual (tumor) epithelial cells. We achieved an F1-score of 0.895 on a hold-out test set and 0.827 on an external reference set from a different center. We envision this segmentation as being the first part of a fully automated prostate cancer detection and grading pipeline.

**Index Terms**—deep learning, computational pathology, digital pathology, prostate cancer

## I. INTRODUCTION

WITH 1.1 million new diagnoses every year, prostate cancer (PCa) is the most common cancer in men in developed countries [1]. PCa develops from genetically damaged glandular epithelium, resulting in altered cellular proliferation patterns. In the case of high-grade tumors, the glandular structure is eventually lost and strands of (individual) cells can be observed instead [2].

The histological grade in PCa is formally defined in the Gleason grading system [3], and is a powerful prognostic

W. Bulten, P. Bándi, G. Litjens and J. van der Laak are with the Diagnostic Image Analysis Group and the Department of Pathology, Radboud University Medical Center, 6500HB Nijmegen, The Netherlands (e-mail: wouter.bulten@radboudumc.nl).

J. Hoven, R. van de Loo and C. Hulsbergen-van de Kaa are with the Department of Pathology, Radboud University Medical Center, 6500HB Nijmegen, The Netherlands

J. Lotz and N. Weiss are with Fraunhofer MEVIS, Lübeck, Germany.

B. van Ginneken is with the Diagnostic Image Analysis Group and the Department of Radiology and Nuclear Medicine, Radboud University Medical Center, 6500HB Nijmegen, The Netherlands

marker. It is determined by pathologists on hematoxylin and eosin (H&E) stained tissue specimens. The grade is based on the architectural growth patterns of the tumor which are assigned a number between 1 and 5, with increasing numbers corresponding to a decrease in histological differentiation, and, typically, worse prognosis [4].

The identification and grading of prostate cancer can be time consuming and tedious for pathologists, as all individual cancer foci within a surgical specimen or biopsy have to be analyzed. This is compounded by the fact that prostate cancer is generally a multi-focal disease and that surgical specimens can consist of anywhere between 8 - 15 sections. Although nowadays, thanks to the advent of whole-slide scanning systems, pathologists can perform their diagnoses on a computer screen instead of using a microscope, this has not directly helped them to perform more efficient or accurate diagnostics. However, computer-aided diagnostic tools based on deep learning and convolutional neural networks have shown promise in improving the accuracy and efficiency of histopathological diagnosis [5].

Deep learning methods that try to detect or grade cancer from scanned tissue slides are typically trained using a set of annotated regions as the reference standard. As these algorithms learn from training data, the quality of the output is directly linked to the quality of the training samples. Ideally, training samples for detecting and grading PCa consist of individually outlined glands. However, outlining PCa requires extensive expert knowledge due to the large differences between and within Gleason grades. In addition, annotating individual cells of high grade PCa is practically infeasible due to the mixture of glandular, stromal and inflammatory components. Therefore, tumor annotations made by pathologists are often coarse and contain large amounts of non-relevant tissue which adds noise to the reference standard and, subsequently, limits the potential of deep learning methods.

We propose a method to automatically improve the detail of PCa annotations by pathologists by dividing digitized tissue into relevant and non-relevant tissue on a pixel-by-pixel basis, in this case epithelial versus other tissues. Such a system can help improve the detail of coarse cancer or grade annotations, but can also be useful by itself in highlighting areas containing epithelial cells as regions of interest for pathologists.

To train our system, we employed a novel two-step approach. First, we trained a convolutional network to segment epithelium in immunohistochemically (IHC) stained tissue

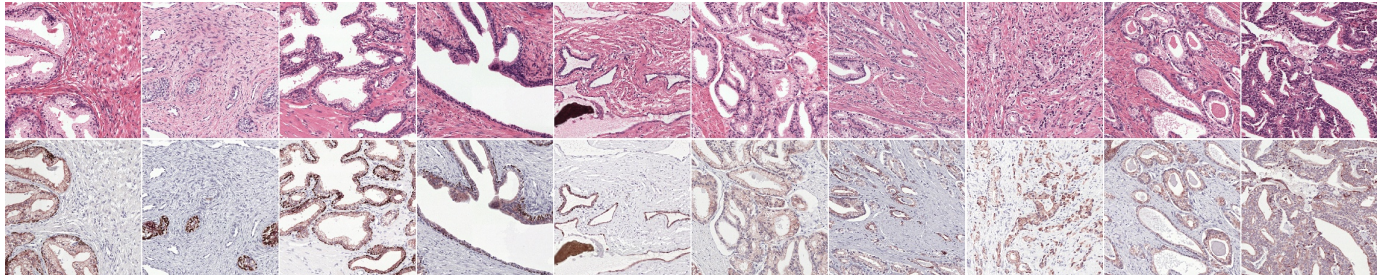


Fig. 1: Dataset examples (first row H&E, IHC second). Our restaining procedure (instead of using consecutive slides) results in perfectly matching slides. The first five columns show benign epithelium, the last five show various grades of PCa.

sections applying an epithelial marker. By applying color deconvolution and subsequent recognition of positively stained pixels, we were able to have ample training data while obviating the cumbersome and imprecise process of manually annotating epithelial regions [6], [7]. Registration was used to map the network’s output to the H&E version of the specimens which were subsequently used as training input for our final model. Our automated segmentation is not only useful as a tool for pathologists, we particularly envision this segmentation as being the first part of a fully automated prostate cancer detection and grading pipeline.

The rest of the paper is organized as follows: in Section II we discuss existing methods for segmenting epithelial tissue. The materials that are used are described in Section III. We discuss our proposed method in Section IV. In section V we show our results and discuss these further in Section VI.

## II. RELATED WORK

Existing research on segmenting epithelial tissue has shown promise in PCa specimens. In [8] a support vector machine was used to distinguish between stroma and epithelial glands and applied to a dataset of 20 patients containing specimens of Gleason grade 3 and 4. Hand crafted features, based on intensity and spatial relationship of pixels, were derived from H&E specimens that had been preprocessed using color deconvolution. In [9] Bayesian classifiers are used to segment glands, relying on the presence of lumen in the glands. The segmentation was applied to Gleason grade 3 and 4, and benign tissue samples; not on the less common but more aggressive pattern 5. Gleason grade 5 can express in the form of single-cell strands or nests, or solid sheets (with or without central necrosis) of malignant cells with no or minimal lumen formation; obviously, this could hinder a segmentation method that relies on the presence of lumina. The authors of [10] employed a multi-step approach based on logistic regression to segment epithelium, distinguishing between glands, lumen, peri-acinar retraction clefting and stroma. Both [8] and [9] used the segmentation results as a first step towards automated Gleason grading.

Advances in deep learning have resulted in new methods for performing segmentation. Deep learning methods generally outperform hand crafted features on segmentation tasks in digital pathology. For example [11] shows the merit of deep learning based segmentation on H&E and IHC stained breast and colon tissue specimens.

Previously, we performed a pilot study on epithelium segmentation using 30 radical prostatectomy slides [12]. We achieved a F1 score of 0.82 using a 4-layer-deep U-Net on a small test set. This dataset consisted of manually annotated areas and we found that the performance of our network capped due to errors in the reference standard. Moreover, a low number of samples, in particular few high grade PCa specimens, limits the applicability to daily practice.

Most of the existing studies on epithelium segmentation in prostate suffer from small datasets or focus on a subset of the occurring grades. In this paper we did not exclude any Gleason grades or gland morphology.

## III. MATERIALS

We selected a cohort of 102 patients who underwent a radical prostatectomy at the Radboud university medical center (Radboudumc) between 2006 and 2011. Patients who received adjuvant therapy before surgery were excluded. From each prostatectomy, we selected one formalin fixated paraffin embedded tissue block based on the Gleason grades reported in the original pathologist’s report. Based on the reported grades, we determined the Gleason grade group [13] for each block (Table I). As a tissue block can contain multiple grades we also reported the individual occurrences of each grade. Of all tissue blocks, 24% contained a region with grade 2, 69% with grade 3, 63% with grade 4 and 33% with grade 5. Due to selective oversampling, the incidence of high grade tumors (grades 4 and 5) is relatively higher than in clinical practice. This oversampling allows us to explicitly investigate the performance of deep learning based epithelium segmentation algorithms on high-grade PCa, in which such segmentation is most challenging.

TABLE I: Overview of case grading from original pathologist’s report on section level (using grade group) and on individual grade.

Set	# slides	Grade group (Section)					Grade (Individual)			
		1	2	3	4	5	2	3	4	5
Train set	62	24	10	11	3	14	12	44	40	22
Test set	40	15	6	7	3	9	12	26	24	12
Total	102	39	16	18	6	23	24	70	64	34

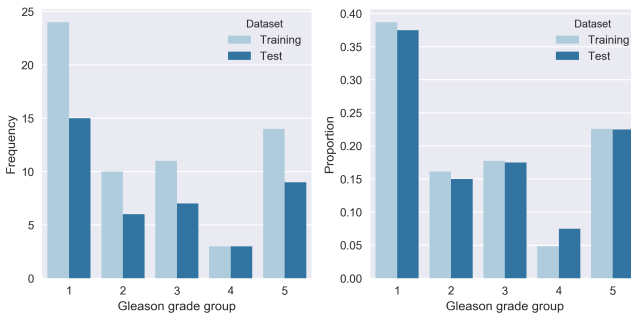


Fig. 2: Distribution of Gleason grade groups for each case in our dataset as reported in the original pathologist's report (N=102).

From each block a new section was cut, stained with H&E and scanned using a *3DHistech Pannoramic Flash II 250 scanner*. After scanning, the tissue was destained, restained using immunohistochemistry, and scanned again. All slides were scanned at 20x magnification (pixel resolution  $0.24\ \mu\text{m}$ ). We used two markers for the immunohistochemistry: CK8/18 (using DAB) to mark all glandular epithelial tissue (benign and malignant), and P63 (using NovaRED) for the basal cell layer, which is normally present in benign glands but not in malignant glands. This procedure resulted in an H&E and IHC whole-slide image (WSI) pair for each patient. Although the slide pairs were made from the same glass slide, minor alignment errors and tissue deformations were still present due to the restaining procedure.

The 102 scanned slide pairs were split into two sets: a training set (62) and a test set (40). The slides were distributed over the sets at random while stratifying for Gleason grade group (Figure 2). The test set was used as a hold-out set and not used during training or model optimization.

#### A. Hold-out test set

For each IHC slide in the test set, a trained non-expert divided each WSI in four sections: two containing tumor and two containing only benign epithelium. From each of these four regions, we extracted an area of  $2500 \times 2500$  pixels randomly at 10x magnification. If there was either no tumor or benign region available, an additional region from the other category was selected. This method resulted in 160 regions.

The tumor regions were individually graded by an experienced pathologist (C.A.H.K) with subspecialty uropathology, without using the original patient's record. We recorded the primary, secondary and tertiary (if present) grade for each region (Figure 3). The reported grades were not necessarily identical to those from the patient records; the selected regions contained a subset of the slide and were extracted from a newly cut section. The Gleason grade group was based on the ISUP scoring system for biopsies (most prevalent plus highest grade).

#### B. External test set

The authors of [8] made their dataset available to use for external validation. This set consists of 224  $1500 \times 1500$  pixels

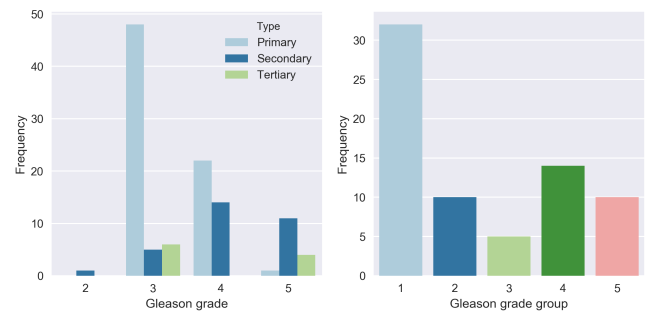


Fig. 3: Gleason grades of tumor regions in the hold-out test set (N=71). Showing individual occurrences (left, 1-3 per region) and grade groups on region level (right).

tiles sampled from 20 digitized WSIs (pixel resolution  $0.5\ \mu\text{m}$ ) of H&E prostatectomy specimens containing Gleason grades 3 and 4. The tiles were already annotated by two pathologists and each pixel labeled as stroma, benign epithelium, Gleason 3 or Gleason 4. Glands were annotated as a whole, including the lumen. We combined the annotations of benign epithelium and the two PCa grades into a single epithelium class.

## IV. METHODS

We took a two-step approach to train a system for segmentation of epithelial tissue on H&E histopathology. First, we circumvented the challenge of manually annotating tissue by generating precise training data using immunohistochemistry and training a network on IHC. Then we transferred the output of the first network to H&E and trained the final segmentation network. Our networks were built using *Keras* [14] and *Tensorflow* [15].

#### A. Slide preparation

We applied a pre-trained tissue-background segmentation network [16] to all slides in order to exclude areas not containing tissue from further analysis. Next, color deconvolution was applied to all WSIs in our training set [6], [7]. The resulting P63/CK8-18 channel was then converted to a binary mask by thresholding. Small errors were removed automatically using binary closing and opening. The resulting masks were not perfect due to imperfections and intensity changes in the stain, scanning artifacts and non-specific staining; e.g. corpora amylacea and debris inside the glands are regularly stained brown and are therefore present in the deconvolution mask.

For our hold-out test set, three trained non-experts reviewed the sampled test regions and manually updated the color deconvolution mask, removing any artifacts or updating incorrectly labeled tissue.

#### B. Training a CNN on IHC

Due to time-constraints, it was unfeasible to manually correct all individual color deconvolution masks to be used for training. Instead, we trained a deep convolutional network to perform the mapping from a P63/CK8-18 slide to a binary epithelium mask. We selected 25 slides from our training set

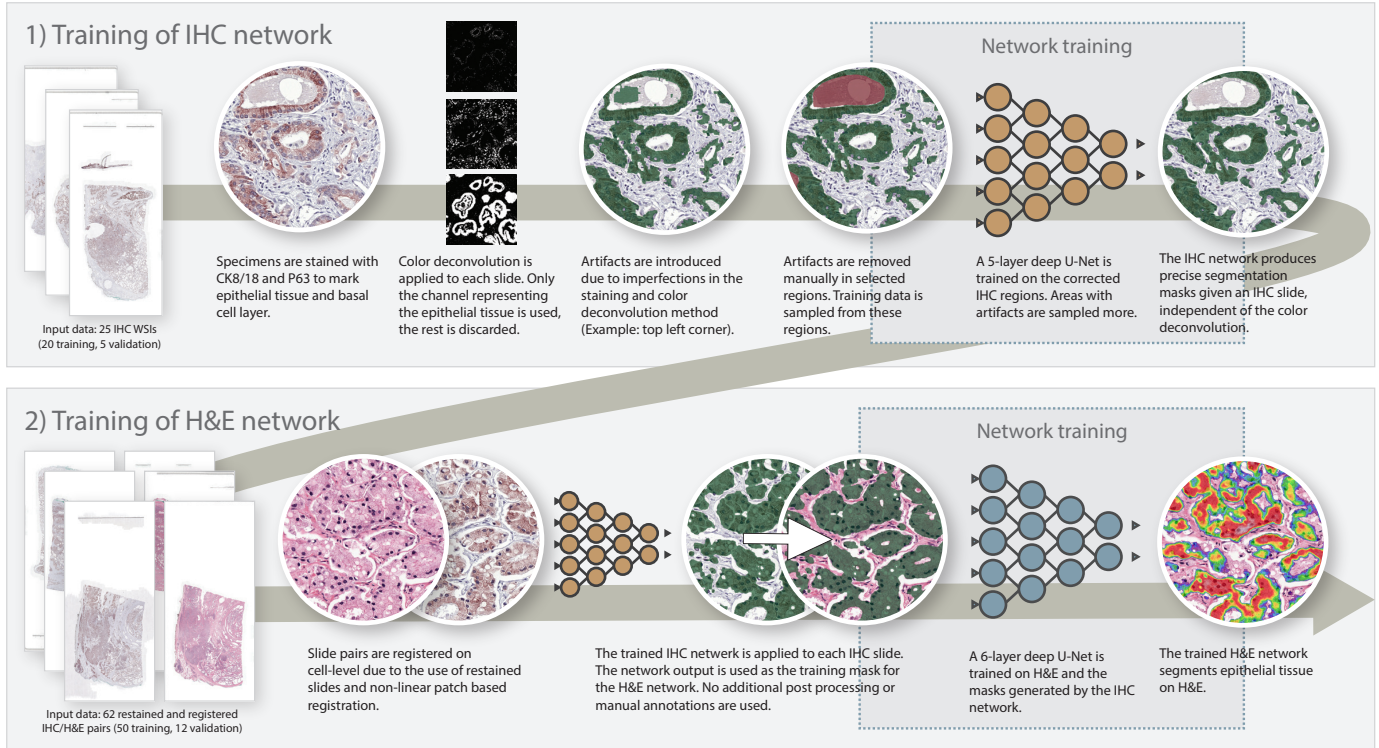


Fig. 4: Overview of methodology. We first train a network (1) on a subset of our IHC training data. The segmentations produced by this first network are then transferred to H&E and used to train the final network (2).

to train this first network (20 for training, 5 for validation). On each slide we outlined a tissue region covering roughly 50% of the WSI in which three trained non-experts removed all the errors in the color deconvolution mask by hand.

We trained a five-level-deep U-Net [17] on the selected regions to segment epithelial tissue in IHC slides. We followed the original U-Net model architecture, but added additional skip connections within each layer block, and used up-sampling operations in the expansion path. The network was trained using randomly sampled patches with a size of  $512 \times 512$  (pixel resolution  $0.48 \mu\text{m}$ ) and a batch size of 1. Regions with annotated artifacts and corpora amylacea were oversampled to lower the number of false positives. Adam optimization was used with  $\beta_1$  and  $\beta_2$  set to 0.99, and a learning rate of 0.0005. The learning rate was halved after every 5 consecutive epochs without improvement on the validation set.

During training, we applied data augmentation to prevent overfitting and to improve the model's generalization. The following augmentations were used: flipping, rotation, additive Gaussian noise, Gaussian blurring and changes in saturation, contrast and brightness. After training, the model was applied to all IHC WSIs in our training set. A binary mask was created from each slide using the argmax of the network output.

### C. Registration

The H&E slides were registered to the IHC slides using a nonlinear image registration method based on a method described previously [18]. Since both slide images showed the

same object with different stains, they were already approximately aligned. However, additional nonlinear deformations are caused by the chemical treatment during restaining and/or the slide scanning procedure and needed to be compensated for.

The registration pipeline consisted of: conversion of RGB images to gray-scale  $\rightarrow$  parametric (affine) registration  $\rightarrow$  non-parametric registration (NGF distance measure [19], curvature regularizer [20])  $\rightarrow$  patch-based registration (NGF, curvature). The method to merge the patches has been extended as follows: Instead of averaging the deformation patches, an optimization problem is solved that balances data-fit and global deformation regularization in the overlap region.

### D. Training a CNN on H&E

The training masks generated by the IHC network matched the H&E slides as a result of the registration step; 50 were used for training and 12 for validation. We found that increasing the depth of the U-Net lowered the number of misclassified corpora amylacea on H&E. Therefore, for the H&E segmentation we trained a six-level-deep U-Net in comparison to the five-level-deep IHC network. To limit the parameter count caused by the added level we lowered the amount of filters for each level. The same extensions as used in the U-Net for the IHC stained images were applied. The network was trained using patches with a size of  $1024 \times 1024$  (pixel resolution  $0.48 \mu\text{m}$ ) and a batch size of 1. Adam optimization was used with  $\beta_1$  and  $\beta_2$  set to 0.99, and a learning rate of 0.0005. The learning rate was halved after every 10 consecutive epochs without improvement on the validation set.

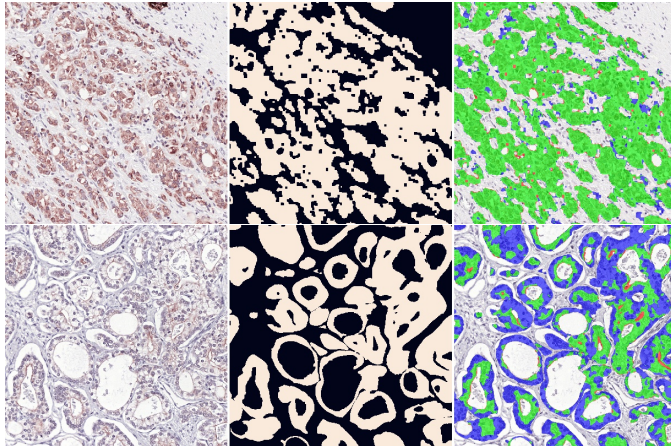


Fig. 5: Zoomed-in examples ( $1000 \times 1000$  crop) of the hold-out test set: IHC version (left), ground truth (middle) and segmentation of the IHC network (right). Green pixels show true positive, red false positive and blue false negative. The first row shows a perfect segmentation. In regions where the stain is light or absent the performance degrades (bottom row).

Only the binary segmentation masks generated by the IHC network were available for training. We did not correct the masks manually. This meant that the sampling technique used for training the IHC network could not be applied to the H&E network. Instead we sampled uniformly over the classes. To force the network to learn small areas of epithelium, e.g. in cases of Gleason 5, we weighted the loss of each pixel based on the class occurrence within a patch. As a result, even patches with only small individual tumor cells were picked up by the network due to a higher loss contribution.

#### E. Evaluation on the hold-out test set

After training we determined the most optimal segmentation threshold for the H&E U-Net based on the manually corrected regions of our training set. The network was then applied to all WSIs of our hold-out set and evaluated within the randomly selected regions. No further post-processing was performed.

#### F. Evaluation on the external test set

The annotations of the external set were coarse and on gland-level (i.e. including the lumina) and did not match the output of our network. In accordance with the method used in the original paper, we removed the background from the color-normalized images of the external test set [8]. Lumina (consisting of pixels which are classified as background pixels) were not used in computing the scores. We then fed the images to our trained H&E network. We did not optimize our network on this external set and used the threshold obtained from our own training set. As such, the results on the external test set can be considered a true estimate of the generalization capacity of our H&E network.

## V. EXPERIMENTAL RESULTS

We evaluated both the IHC and H&E networks on the regions from, respectively, the IHC and the H&E WSIs from

TABLE II: Segmentation results on the hold-out test set.

Regions	N	F1 score mean (min, max)	Acc.	Jaccard
<b>IHC network</b>				
All regions	160	$0.914 \pm .09$ (0.353, 0.980)	0.952	0.851
Benign	89	$0.941 \pm .05$ (0.710, 0.980)	0.980	0.892
Cancer	71	$0.879 \pm .11$ (0.353, 0.975)	0.917	0.799
<b>H&amp;E network</b>				
All regions	160	$0.895 \pm .05$ (0.673, 0.957)	0.941	0.813
Benign	89	$0.909 \pm .04$ (0.774, 0.957)	0.967	0.836
Cancer	71	$0.878 \pm .05$ (0.673, 0.955)	0.909	0.785
Grade group 1	32	$0.887 \pm .03$ (0.816, 0.938)	0.924	0.798
Grade group 2	10	$0.886 \pm .03$ (0.855, 0.930)	0.897	0.797
Grade group 3	5	$0.892 \pm .03$ (0.835, 0.921)	0.912	0.807
Grade group 4	14	$0.889 \pm .06$ (0.727, 0.955)	0.908	0.805
Grade group 5	10	$0.816 \pm .07$ (0.673, 0.907)	0.875	0.695

TABLE III: Comparison of results on the external test set.

Network	Acc.	F1	Jaccard
Gertych et al. [8]	-	-	$0.595 \pm 0.15$
Our method	$0.861 \pm 0.07$	$0.827 \pm 0.14$	$0.724 \pm 0.16$

the hold-out test set. The thresholded network output was compared with the ground truth (color deconvolution masks with manual corrections). We report pixel-based accuracy, F1-score and Jaccard index using epithelium as the positive label (Table II).

#### A. Segmentation performance on IHC

The IHC network achieved an overall F1 score of 0.914. Given a minimum F1 score of 0.353 and a maximum of 0.980, the range of scores was high. Some regions of our test set suffered from an overall low stain quality or contained areas where the epithelium reacted less to the stain. We observed that a lower stain intensity resulted in a lower performance (Figure 5). As the H&E network was trained on the output of the IHC network we considered the IHC performance as an upper bound for the performance of the H&E network.

#### B. Segmentation performance on H&E

The H&E network achieved an overall F1 score of 0.895. The score on benign tissue (F1 0.909) was slightly higher than on tumorous areas (F1 0.878). A decline in performance was observed in regions with higher Gleason grades. Regions with Gleason grade group 5 had an F1 score of 0.816. Several regions are displayed in Figure 6.

The score of the H&E network was comparable to that of the IHC network, showing that, given this training data, the network achieved an almost optimal performance. Even more, the minimal performance of the H&E network was higher than the minimum of the IHC network (0.673 versus 0.353). Outliers that were present in the results of the IHC network were not present in the results of the H&E network.

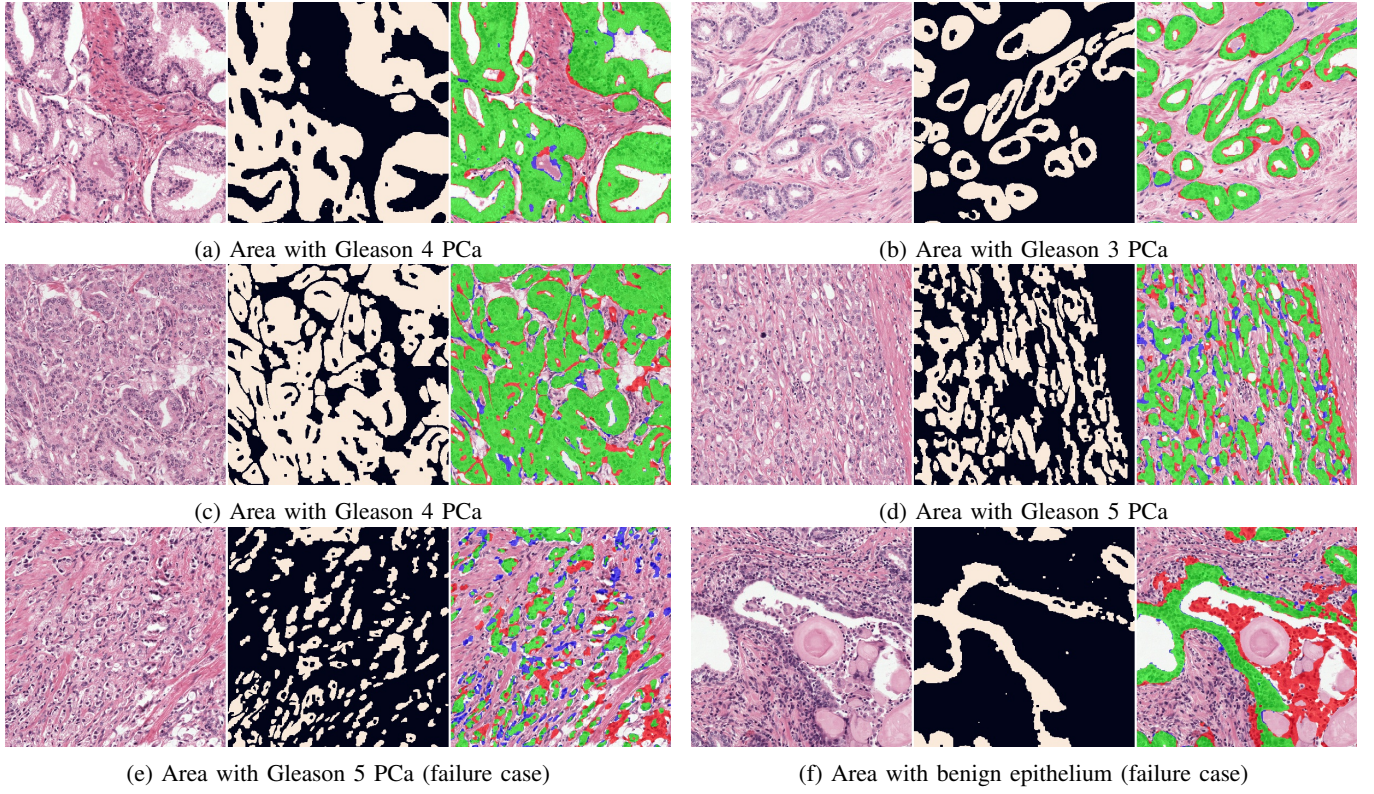


Fig. 6: Zoomed-in example regions ( $1000 \times 1000$  crop) from the hold-out test set with H&E (left), ground truth (middle) and network segmentation (right). Green pixels show true positive, red false positive and blue false negative. The top two rows displays two cases (a, b, c, d) of PCa where the network segments the epithelial tissue almost perfectly. In the bottom row two failure cases are shown: a case of high grade PCa (c) and a benign region (d) where debris inside the gland is segmented.

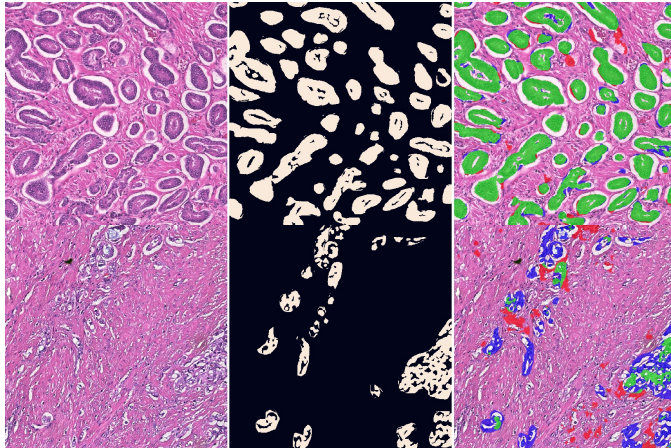


Fig. 7: H&E network applied to cases from the external test set. Top row shows an example of a good segmentation. The bottom row shows a case of undersegmentation.

### C. Segmentation performance on external dataset

On the external set our network achieved an F1 score of 0.827 (Table III, Figure 7). This is lower than on our hold-out test set, but within expectations due to the differences in staining and image resolution. With a Jaccard score of 0.724 we achieved a higher score than the original method published in [8], which had a Jaccard score of 0.595.

## VI. DISCUSSION

We developed a deep learning based system that segments epithelial tissue in H&E-stained whole-slide prostatectomy images. Our system produces cell-level segmentations and is able to segment both intact glands as well as individual (tumor) epithelial cells. A common problem when training deep learning models for scanned histology sections is the absence of a precise ground truth. We circumvented this problem by restaining our slides with an epithelial and basal cell layer marker. Using color deconvolution and a separately trained network we were able to exhaustively annotate our complete training set with only a minimal amount of manual labor. This technique works especially well for annotating small instances of epithelium, e.g. cases of Gleason 5 PCa, that would most likely be missed by human annotators. Moreover, use of specific markers renders our ground truth less subjective compared to manually produced annotations on H&E slides (even in inflamed or poorly differentiated areas). On an external test set we see a drastic performance improvement compared to the original method, showing the generalization capacity of our network, even on images from an external center. Of notice is that the original method we compare against was trained on the external test dataset (in cross-validation), whereas our network has never seen this data before.

In contrast to other previous work, we assess the perfor-

mance of our algorithm across all Gleason grades, including the notoriously difficult Gleason grade 5. Although we do obtain the lowest score on this pattern (F1-score of 0.816), this score is still high especially given the poorly differentiated character of high Gleason grades, and the first benchmark on these grades. To allow others to compare their algorithms against ours we have decided to release our test data and all the H&E WSIs publicly, including both the test and training slides.

Our work also has some limitations. The method to establish the training labels is not perfect. The IHC network is only trained on a limited set of WSIs and is therefore not able to overcome all problems caused by stain variability and presence of scan and tissue artifacts. Especially corpora amylacea or other debris inside glands, which are often stained by the epithelial marker, are a source of errors. Epithelium glands are also missed by the network when the stain is light or absent. Subsequently, misclassified areas on the IHC slides are transferred to the training data of the H&E network. Many of these errors are overcome by the H&E network due to the larger size of the H&E training set, which results in a much higher minimum performance with an F1-score of 0.673 vs. 0.353 for the IHC network.

The type of misclassifications is also influenced by the chosen magnification level. A low magnification is sufficient for segmenting intact glands, and could potentially help with lowering the number of artifacts as the network can learn high level shapes of the tissue. However, segmenting individual epithelial cells, especially in the case of high grade PCa, requires input patches with enough detail to be able to distinguish those cells from the surrounding stroma. We deliberately chose a high magnification level to improve the performance on high grade PCa. In future work it might be fruitful to investigate multi-scale approaches to tackle this issue.

We observe that the segmentation performance of our H&E network approaches that of the IHC network, which is used to generate the training reference for the H&E network. As a result, there is only a limited amount of improvement possible without further refining the training data. Annotating specific regions that are troublesome and retraining the IHC network on these regions could further boost the performance of the H&E network. However, one needs to consider that for some cells it is simply impossible to assess their class using the H&E stain alone, especially in areas with active inflammation. As such a perfect segmentation does not exist.

We see the development of an accurate epithelium segmentation network as the first part of a fully automated prostate cancer detection and grading pipeline. More specifically, the epithelium segmentation can be used to precisely outline potential cancer regions, and in combination with coarse tumor annotations result in highly detailed annotations of PCa. We intend to leverage this to develop highly accurate PCa segmentation networks in the near future.

#### ACKNOWLEDGMENT

This study was financed by a grant from the Dutch Cancer Society (KWF), grant number KUN 2015-7970. The authors

would like to thank Milly van den Warenburg and Nikki Wissink for their help making the manual annotations.

#### REFERENCES

- [1] L. A. Torre, F. Bray, R. L. Siegel, J. Ferlay, J. Lortet-tieulent, and A. Jemal, "Global Cancer Statistics, 2012," *CA: a cancer journal of clinicians.*, vol. 65, no. 2, pp. 87–108, 2015.
- [2] S. W. Fine *et al.*, "A contemporary update on pathology reporting for prostate cancer: Biopsy and radical prostatectomy specimens," *European Urology*, vol. 62, no. 1, pp. 20–39, 2012.
- [3] J. I. Epstein, "An Update of the Gleason Grading System," *Journal of Urology*, vol. 183, no. 2, pp. 433–440, 2010.
- [4] J. I. Epstein *et al.*, "The 2005 International Society of Urological Pathology (ISUP) consensus conference on Gleason grading of prostatic carcinoma," *American Journal of Surgical Pathology*, vol. 29, no. 9, pp. 1228–1242, 2005.
- [5] G. Litjens *et al.*, "Deep learning as a tool for increased accuracy and efficiency of histopathological diagnosis," *Nature Scientific Reports*, vol. 6, p. 26286, 2016.
- [6] A. C. Ruifrok and D. A. Johnston, "Quantification of histochemical staining by color deconvolution," *Analytical and Quantitative Cytology and Histology*, vol. 23, pp. 291–299, 2001.
- [7] D. J. Geijs, M. Intezar, J. A. W. M. van der Laak, and G. J. S. Litjens, "Automatic color unmixing of IHC stained whole slide images," in *Medical Imaging 2018: Digital Pathology*, vol. 10581, 2018.
- [8] A. Gertych *et al.*, "Machine learning approaches to analyze histological images of tissues from radical prostatectomies," *Computerized Medical Imaging and Graphics*, vol. 46 Pt 2, pp. 197–208, Dec. 2015.
- [9] S. Naik, S. Doyle, M. Feldman, J. Tomaszewski, and A. Madabhushi, "Gland Segmentation and Computerized Gleason Grading of Prostate Histology by Integrating Low- , High-level and Domain Specific Information," in *Proceedings of 2nd Workshop on Microscopic Image Analysis with Applications in Biology*, 2007, pp. 1–8.
- [10] M. Singh, E. M. Kalaw, D. M. Giron, K.-T. Chong, C. L. Tan, and H. K. Lee, "Gland segmentation in prostate histopathological images," *Journal of Medical Imaging*, vol. 4, no. 2, p. 027501, 2017.
- [11] J. Xu, X. Luo, G. Wang, H. Gilmore, and A. Madabhushi, "A deep convolutional neural network for segmenting and classifying epithelial and stromal regions in histopathological images," *Neurocomputing*, 2016.
- [12] W. Bulten, C. A. Hulsbergen-vandeKaa, J. van der Laak, and G. J. S. Litjens, "Automated segmentation of epithelial tissue in prostatectomy slides using deep learning," in *Medical Imaging*, ser. SPIE, vol. 10581, 2018.
- [13] J. I. Epstein *et al.*, "A contemporary prostate cancer grading system: A validated alternative to the gleason score," *European urology*, vol. 69, pp. 428–435, Mar 2016.
- [14] F. Chollet *et al.*, "Keras," <https://github.com/keras-team/keras>, 2015.
- [15] M. Abadi *et al.*, "TensorFlow: Large-scale machine learning on heterogeneous systems," 2015, software available from tensorflow.org. [Online]. Available: <https://www.tensorflow.org/>
- [16] P. Bandi *et al.*, "Comparison of different methods for tissue segmentation in histopathological whole-slide images," in *IEEE International Symposium on Biomedical Imaging*, 2017, pp. 591–595.
- [17] O. Ronneberger, P. Fischer, and T. Brox, "U-net: Convolutional networks for biomedical image segmentation," in *Medical Image Computing and Computer-Assisted Intervention*, ser. Lecture Notes in Computer Science, vol. 9351, 2015, pp. 234–241.
- [18] J. Lotz *et al.*, "Patch-based nonlinear image registration for gigapixel whole slide images," *IEEE Transactions on Biomedical Engineering*, vol. 63, no. 9, pp. 1812–1819, 2016.
- [19] E. Haber and J. Modersitzki, "Intensity gradient based registration and fusion of multi-modal images," *Methods of Information in Medicine*, vol. 46, no. 3, pp. 292–299, 2007.
- [20] B. Fischer and J. Modersitzki, "Curvature based image registration," *Journal of Mathematical Imaging and Vision*, pp. 81–85, 2003.